pretation above. This change is similar to that predicted (*1*) but is apparently delayed by ~2 years, which suggests that GCMs may merit refinement. An unavoidable deficiency in present Titan GCMs is the lack of surface topography, so atmospheric torque is assumed to be attributable only to skin friction. However, it is known that there are kilometer-high mountain chains on Titan (*22*) and that a pressure field can exert a torque on the surface via pressure differences across mountain chains [e.g., (*2*, *23*)]. Another assumption that bears further examination is that of complete decoupling from the ocean. Friction at the bottom of the ice layer would allow the ocean to act as another angular momentum reservoir, generally providing a higher apparent moment of inertia than the ice crust alone, but likely increasing the complexity of the spin history.

Regardless of the details, an important and robust conclusion of this study is that the spin period can be expected to vary substantially over time scales of a few years, and indeed other data (*8*) show that the rate of change of spin rate must have been different over the past couple of decades. Taking the phase-lagged model as a guide, Titan's spin should peak during the proposed extended mission (2008–2010) and then begin to decline. We predict that other anticipated Cassini results, such as determination of the tidal Love number k_2 (*12*) from radio tracking (*24*), will be consistent with an internal aqueous ocean. Induced magnetic fields in such an ocean, which might independently constrain the ice thickness and ocean conductivity (*25*), will be difficult to detect on Cassini flybys, although a future dedicated Titan orbiter/lander mission could succeed. Such a mission would itself provide new rotation measurements of this body, which combines the astrobiological appeal of a subsurface water ocean on an organic-rich icy satellite with solid-body rotation effects driven by atmospheric dynamics that are more profound than those observed on the terrestrial planets.

References and Notes

1. T. Tokano, F. Neubauer, *Geophys. Res. Lett.* **32**, L24203 (2005).
2. R. Hide, N. T. Birch, L. V. Morrison, D. J. Shea, A. A. White, *Nature* **286**, 114 (1980).
3. J. P. Peixoto, A. H. Oort, *Physics of Climate* (AIP Press, New York, 1992).
4. W. M. Folkner, C. F. Yoder, D. N. Yuan, E. M. Standish, R. A. Preston, *Science* **278**, 1749 (1997).
5. J. L. Margot, S. J. Peale, R. F. Jurgens, M. A. Slade, I. V. Holin, *Science* **316**, 710 (2007).
6. B. Stiles *et al.*, *Bull. Am. Astron. Soc.* **39**, 543 (2007).
7. P. Persi de Malmo, L. Iess, G. Picardi, R. Seu, B. Bertotti, *Bull. Am. Astron. Soc.* **39**, 543 (2007).
8. See supporting material on *Science* Online.
9. B. G. Bills, *Icarus* **175**, 233 (2005).
10. P. Goldreich, *Astron. J.* **71**, 1 (1961).
11. R. Greenberg, S. Weidenschilling, *Icarus* **58**, 186 (1984).
12. W. D. Sears, J. I. Lunine, R. Greenberg, *Icarus* **105**, 259 (1993).
13. P. H. Smith *et al.*, *Icarus* **119**, 336 (1996).
14. J. Richardson, R. D. Lorenz, A. McEwen, *Icarus* **170**, 113 (2004).
15. F. Sohl, H. Hussmann, B. Schwentker, T. Spohn, R. D. Lorenz, *J. Geophys. Res.* **108**, 10.1029/2003JE002044 (2003).
16. M. K. Bird *et al.*, *Nature* **438**, 800 (2005).
17. D. J. Stevenson, *Eur. Space Agency Spec. Publ. ESA SP-338* (1992), pp. 29–33.
18. O. Grasset, C. Sotin, F. Deschamps, *Planet. Space Sci.* **48**, 617 (2000).
19. A. D. Fortes, *Icarus* **146**, 444 (2000).
20. C. Zimmer, K. K. Khurana, M. G. Kivelson, *Icarus* **147**, 329 (2000).
21. C. Elachi *et al.*, *Nature* **441**, 709 (2006).
22. J. Radebaugh *et al.*, *Lunar Planet. Sci. Conf.* **XXXVII**, 1007 (2006).
23. R. M. White, *J. Meteorol.* **6**, 353 (1949).
24. N. Rappaport, B. Bertotti, G. Giampieri, J. D. Anderson, *Icarus* **126**, 313 (1997).
25. K. Hand, C. Chyba, *Icarus* **189**, 424 (2007).

26. We thank those who designed, developed, and operate the Cassini/Huygens mission, and in particular our colleagues on the Cassini radar team. Cassini is a joint endeavor of NASA, ESA, and the Italian Space Agency (ASI) and is managed by the Jet Propulsion Laboratory, California Institute of Technology, under a contract with NASA.

Supporting Online Material

www.sciencemag.org/cgi/content/full/319/5870/1649/DC1
Materials and Methods
Figs. S1 to S3
References

11 October 2007; accepted 24 January 2008
10.1126/science.1151639

Chloride-Bearing Materials in the Southern Highlands of Mars

M. M. Osterloo,[1]* V. E. Hamilton,[1] J. L. Bandfield,[2]† T. D. Glotch,[3] A. M. Baldridge,[2]‡ P. R. Christensen,[2] L. L Tornabene,[4] F. S. Anderson[1]

Chlorides commonly precipitate during the evaporation of surface water or groundwater and during volcanic outgassing. Spectrally distinct surface deposits consistent with chloride-bearing materials have been identified and mapped using data from the 2001 Mars Odyssey Thermal Emission Imaging System. These deposits are found throughout regions of low albedo in the southern highlands of Mars. Geomorphologic evidence from orbiting imagery reveals these deposits to be light-toned relative to their surroundings and to be polygonally fractured. The deposits are small (< ~25 km^2) but globally widespread, occurring in middle to late Noachian terrains with a few occurrences in early Hesperian terrains. The identification of chlorides in the ancient southern highlands suggests that near-surface water was available and widespread in early Martian history.

On Earth, chlorides are formed by precipitation from evaporating surfaces (e.g., saline lakes) or groundwater/hydrothermal brines, as volcanic sublimates (e.g., at fumaroles) and by efflorescence (direct crystallization onto sediment grains forming crusts) (*1*). Typically, chloride deposits produced by precipitation have large surface relief and polygonal to blocky morphologies, whereas efflorescence tends to produce thin crusts (*1*). For terrestrial evaporite systems, the most important variable for the resultant brine composition and saline mineral assemblages is the composition of the dilute water at the onset of concentration (evaporation) (*2*). Generally, chlorides in terrestrial settings occur in alkaline environments and are the last minerals to precipitate out of saline brines, preceded by various carbonates, sulfates, and silica. On Mars, saline minerals (including various chlorides) are predicted to form from acidic fluids derived from basaltic weathering (*3*). Geologic environments that contain saline minerals are of key interest to the exobiology community because they are potentially areas of biological activity and chemical sedimentation, which is optimal for the preservation of biological signatures and a high priority for future exploration by orbiting and landed missions (*4*).

Using Mars Odyssey Thermal Emission Imaging System (THEMIS) data (*5*), as well as supporting data from the Mars Global Surveyor (*6*) and Mars Reconnaissance Orbiter (*7*), we have identified a compositional unit on Mars that contains a mineralogical component likely attributable to chloride salts. We initially identified these deposits because of their spectral distinctiveness in false-color, decorrelation stretched (DCS), THEMIS daytime infrared radiance images (*8*). The deposits range in area from ~1 km^2 to ~25 km^2 and generally are topographically lower than the immediate surrounding terrain. The spectrally distinct deposits commonly exhibit irregular outlines (Fig. 1A) and occur less commonly in small craters and sinuous channels (Fig. 1, B to D). Our examination of the THEMIS daytime infrared data set has revealed ~200 of these deposits throughout the low albedo, mid-to-low latitude southern highlands (Fig. 2), corresponding to mid-

[1]Hawaii Institute of Geophysics and Planetology, University of Hawaii, 1680 East-West Road, Honolulu, HI 96822, USA. [2]School of Earth and Planetary Exploration, Arizona State University, Tempe, AZ 85287, USA. [3]Department of Geosciences, Stony Brook University, Stony Brook, NY 11794, USA. [4]Lunar and Planetary Laboratory, University of Arizona, Tucson, AZ 85721, USA.

*To whom correspondence should be addressed. E-mail: osterloo@higp.hawaii.edu
†Present address: Department of Earth and Space Sciences, University of Washington, Johnson Hall 070, Box 351310, Seattle, WA 98195–1310, USA.
‡Present address: Jet Propulsion Laboratory, M/S 183-501, 4800 Oak Grove Drive, Pasadena, CA 91109, USA.

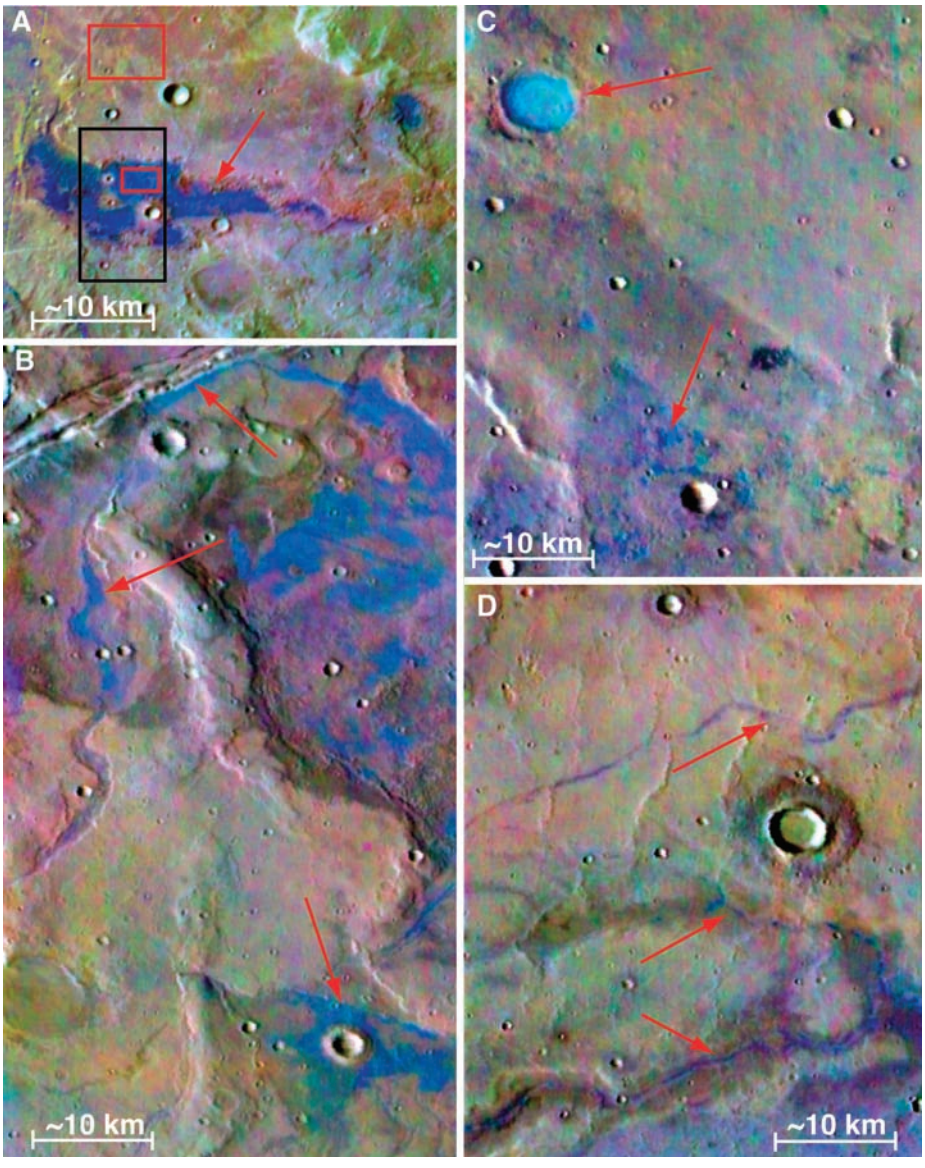

Fig. 1. All images are THEMIS 8/7/5 DCS radiance images. (**A**) I08831002 (~221.0° E, –38.8° N) showing spectrally distinct materials in blue. Red boxes indicate areas averaged for spectral analysis, and the black box indicates HiRISE coverage. (**B**) I07808003 (~205.5°E, –32.7 °N) showing spectrally distinct materials following sinuous paths, abutting Sirenum Fossae, and occurring in low-lying areas near craters. (**C**) I07815002 (~4.1° E, –28.0° N) showing spectrally distinct materials filling a small crater, as well as occurring as patches. (**D**) Spectrally distinct materials following sinuous path in I07830004 (~290.8° E, –34.0° N).

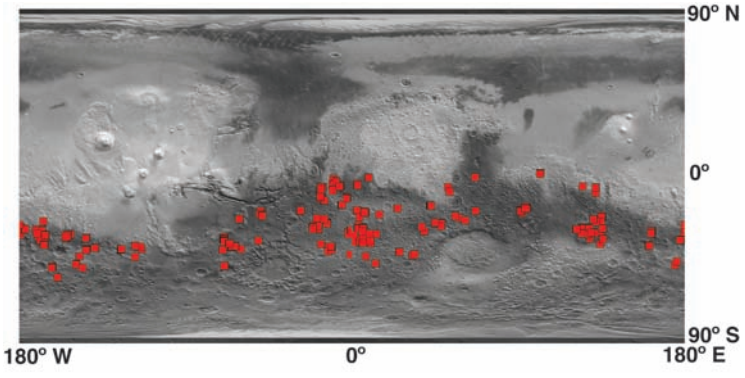

Fig. 2. Global distribution of spectrally distinct materials overlain on TES Lambert albedo and MOLA shaded relief.

Noachian [~3.9 to ~3.8 billion years ago (Gya)] terrains and the Hesperian ridged plains unit (~3.7 to ~3.5 Gya) (*9*).

THEMIS surface emissivity spectra (*10*) of the deposits show that they have a spectral shape that is unlike any previously studied surface type (*11*–*14*). Whereas the regional materials (Fig. 3A) exhibit a basaltic spectral shape, the distinct deposits are characterized by higher emissivity across the 1260 to 900 cm^{-1} range and exhibit a featureless spectral slope toward lower wave numbers. Higher spectral resolution (10 cm^{-1} sampling) Thermal Emission Spectrometer (TES) data can be used to further constrain the mineralogy of these surfaces, although at lower spatial resolution (~3 × 6 km minimum) (*8*). In Terra Sirenum, the spectrum of the spectrally distinct material is similar to that of the surrounding terrain in that it exhibits a shape similar to that of a basalt, but it differs in having a negative spectral slope (Fig. 3B). The basaltic shape is attributable to the large spatial area measured by TES relative to THEMIS, which leads to subpixel mixing and dilution of the spectrally distinct material by the regional basaltic materials. Spectral ratios were used to remove features common to both spectra and derive a residual spectral shape that represents the difference between the two materials (*15*). The resulting ratio spectrum is relatively featureless and slopes toward lower wave numbers, as shown in Fig. 3B. A slight residual "hump" in the ratio spectrum between ~1330 and 830 cm^{-1} resembles the basaltic shape (inverted) and is attributable to a difference in spectral contrast between the two spectra, both of which include basaltic materials. Therefore, we conclude that the spectral character of the spectrally distinct deposits is nearly featureless and inconsistent with previously derived TES surface shapes (*8*, *11*–*14*). Quantitative linear deconvolution and factor analysis/target transformation analyses of the TES data also indicate that phases with weak spectral features and negative slopes are candidates for the component that is responsible for the spectrally distinct materials, although there is no phase in our spectral library [which contains >200 rock and mineral phases, including phyllosilicates and sulfates, (*16*)] that results in a good model fit (*8*).

A negative spectral slope in mid-infrared emissivity spectra can arise from errors in the derivation of temperature in the process of converting radiance (a temperature-dependent parameter) to emissivity (which is independent of temperature) (*8*, *17*). The separation of temperature and emissivity relies on the assumption that the observed radiance represents a single or narrow range of temperatures (e.g., a few degrees K) and that the emissivity of the materials is unity at some point in the spectral range. We find no evidence for large temperature variations at the 100 m/pixel scale of the THEMIS instrument that would introduce such temperature errors (*8*). However, if the observed materials do not exhibit unit emissivity (as assumed at some point in the wavenumber range used to determine the target temper-

ature), incorrect temperatures may be derived during the conversion of radiance to emissivity (*8*). For materials having a maximum emissivity less than unity, the target temperature will be underestimated and a slope will be imparted to the resulting emissivity spectrum (*17*).

Virtually all silicate phases (and most carbonate, sulfate, and oxide phases) exhibit near-unit emissivity at some point in the 1350 to 300 cm^{-1} range used for the TES temperature-emissivity separation (*18*); however, some chlorides have relatively featureless spectra in this range (*8*, *19*, *20*). One or more chlorides as a component of the Martian materials would reduce emissivity, causing incorrect temperature derivation and introducing a slope in the emissivity spectrum. Chloride salts have been identified on Earth in infrared multispectral data on the basis of similar observations; for example, the presence of halite was accurately inferred in Death Valley, California, by a lack of spectral features in high-resolution MODIS (Moderate Resolution Imaging Spectroradiometer)/ASTER (Advanced Spaceborne Thermal Emission and Reflection Radiometer) Airborne Simulator (MASTER) which covers a similar wavelength range as the THEMIS instrument (*8*, *21*). Based on the observed Martian spectra, the assumption of unit emissivity during TES and THEMIS data reduction, the laboratory measurements of the behavior of chloride salts, and similar terrestrial identifications, we interpret these spectrally distinct materials to be chloride-bearing deposits.

Further insight into the nature and origin of the putative chloride-bearing deposits is provided by visible images from THEMIS (*5*), the High Resolution Imaging Science Experiment (HiRISE) (*7*), and the Mars Orbiter Camera (MOC) (*6*), topography from the Mars Orbiter Laser Altimeter (MOLA) (*22*), and thermal inertia from THEMIS nighttime data (*23*). MOC images (~2.95 m/pixel) of the Terra Sirenum deposit and other deposits across the southern highlands show that the chloride-bearing materials are light-toned; in addition, they exhibit patterned-ground and etched-terrain morphologies. Higher spatial resolution (~25.3 cm/pixel) HiRISE images of the materials in Terra Sirenum also show the putative chloride-bearing materials to be light-toned and highly fractured and to have an etched morphology that may indicate cemented aeolian bedforms (Fig. 4, A and B). The chloride-bearing materials appear to have been exposed by erosion of dark materials, which are observed bordering the light-toned deposit (Fig. 4A).

The pervasive polygonal fracturing observed in the HiRISE image is irregular, with variable diameters (Fig. 4B.). The fractures defining the polygons crosscut ridges and valleys and occur along ridge crests, indicating that the surface is an indurated material (Fig. 4C). Thermal inertia derived from THEMIS nighttime infrared observations indicates that the chloride-bearing material in Terra Sirenum has a thermal inertia close to 400 $Jm^{-2}K^{-1}s^{-1/2}$, whereas values for the surrounding terrain are substantially lower (180 to 280) (*23*). The values for the putative chloride-bearing deposits are consistent with a mean particle size of fine gravel (2 to 4 mm) (*24*). However, thermal inertia is not a uniquely interpretable parameter, and values in this range also are consistent with smaller-grained particles that are cemented together (*25*). The latter is consistent with the generally crusty to indurated appearance for the chloride-bearing deposits observed in the MOC and HiRISE imagery.

The relationship between the putative chloride-bearing materials and craters is complex. A number of small (<300 m diameter), highly degraded craters appear to predate the chloride-bearing materials in Terra Sirenum, indicated by polygonal fractures crosscutting the crater rims and sidewalls (Fig. 4C). Larger craters (~300 to 900 m) in the same area appear to have excavated through the materials, covering them with ejecta (Figs. 1A and 4A). In other locations, chloride-bearing materials fill the floors of degraded craters but do not fill nearby, less degraded craters (Fig. 1C). In Terra Sirenum, a small crater ~500 m in diameter shows the light-toned, putative chloride-bearing materials in cross-section and reveals that the stratigraphic unit containing the putative

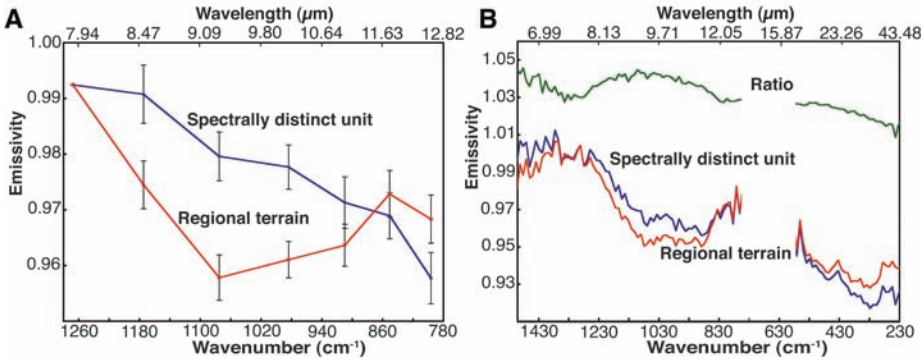

Fig. 3. (**A**) THEMIS surface spectra from image I08831002 in Terra Sirenum. (**B**) TES data for the spectrally distinct materials and the surrounding terrain. The ratio of the spectrally distinct surface to the surrounding terrain is shown at top.

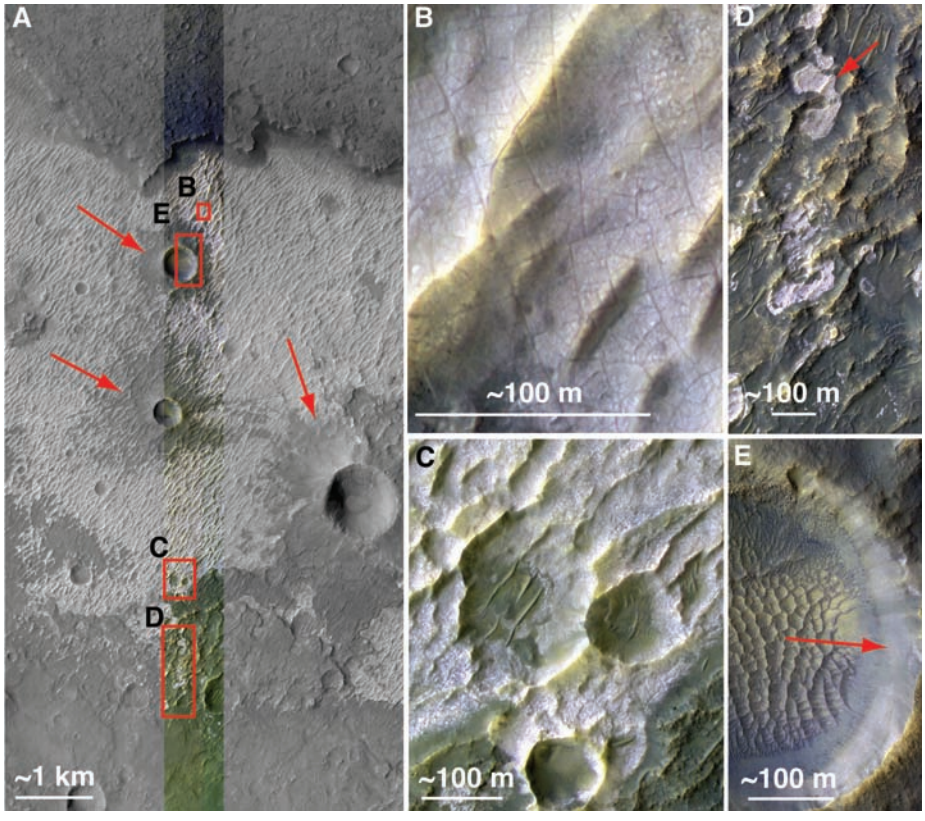

Fig. 4. (**A**) HiRISE image PSP_003160_1410, which includes the location of color data; locations of color inset images are indicated by red boxes. Crater ejecta overlie the light-toned materials, as indicated by the red arrows. (**B**) Polygonal fractures. (**C**) Chloride-bearing material appears to post-date small, degraded craters. (**D**) Small patches of chloride-bearing material with ambiguous stratigraphic relationships. (**E**) Light-toned materials are visible in the wall of this ~500-m-diameter crater.

chloride-bearing materials has a substantial thickness (Fig. 4E) (*8*).

On a global scale, the chloride-bearing materials occur at a wide range of elevations, ranging from roughly –3 to 3 km. MOLA gridded elevation data show that individual deposits not located in crater floors commonly occur in local topographic lows relative to the immediate surrounding terrain. As described previously, many of the deposits occur as small, isolated patches; in conjunction with their locally low elevations, this suggests they most likely represent incontiguous units. Additionally, within a region containing several deposits, the putative chloride-bearing materials may occur at different elevations relative to each other, indicating that the formation postdates the stratigraphy, although it may also suggest the presence of multiple units in the stratigraphy.

On the basis of our observations, a number of inferences can be drawn about how the putative chloride-bearing deposits might have formed on the Martian surface. The widespread distribution of the deposits suggests that the climatological/hydrological conditions that facilitated their deposition were global in scale. However, ocean-scale bodies of water would appear to be inconsistent with the deposits' concentration in the cratered southern highlands. Alone, local-scale processes such as fumarolic activity are unlikely to produce the observed global distribution and differing morphologies of the deposits. Similarly, efflorescence alone does not account for the observed polygonal morphologies of the deposits, which are more consistent with desiccation cracks in thick salt deposits forming through precipitation. The occurrences of putative chloride-bearing materials in crater floors and in association with sinuous channels suggest that many of the putative chloride-bearing materials were precipitated from brines. Crater floors are ideal locations for ponding and evaporation of brines trapped from surface runoff or by the intersection of groundwater with the surface. Additionally, impact melting and mobilization of subsurface groundwater (or ground ice) could also be a viable mechanism for the production of chlorides. Based on our observations, we believe that the majority of the deposits were formed by chloride precipitation processes, although it is likely that in various locations, some of the materials are efflorescent salts or volcanic sublimates or were precipitated from hydrothermal brines (*8*). Locations where the stratigraphic relationship between the putative chloride-bearing materials and surrounding terrain is not clear (Fig. 4D) may be candidates for reactivation and/or modification of the original deposits by efflorescence.

The abundance of these deposits indicates that the formation of chloride salts on Mars has been an important process (*26*, *27*). The deposition of widespread chloride-bearing materials in the ancient southern highland terrains of Mars is further evidence of the presence of extensive reservoirs of surface and/or subsurface groundwater in the planet's early history (*8*).

References and Notes

1. T. M. Goodall, C. P. North, K. W. Glenn, *Sedimentology* **47**, 99 (2000).
2. H. P. Eugster, L. A. Hardie, in *Saline Lakes*, A. Lerman, Ed. (Springer-Verlag, New York, 1978), pp. 237–293.
3. N. J. Tosca, S. M. McLennan, *Earth Planet. Sci. Lett.* **241**, 21 (2006).
4. J. D. Farmer, D. J. Des Marais, *J. Geophys. Res.* **104**, 26977 (1999).
5. P. R. Christensen *et al*., *Space Sci. Rev.* **110**, 85 (2004).
6. M. C. Malin *et al*., *J. Geophys. Res.* **97**, 7699 (1992).
7. A. S. McEwen *et al*., *J. Geophys. Res.* **112**, E05S02 (2007).
8. Materials and methods are available as supporting material on *Science* Online.
9. W. K. Hartmann, G. Neukum, *Space Sci. Rev.* **96**, 165 (2001).
10. J. L. Bandfield, A. D. Rogers, M. D. Smith, P. R. Christensen, *J. Geophys. Res.* **109**, E10008 (2004).
11. J. L. Bandfield *et al*., *Science* **287**, 1626 (2000).
12. M. T. Hoefen *et al*., *Science* **302**, 627 (2003).
13. P. R. Christensen *et al*., *J. Geophys. Res.* **105**, 9623 (2000).
14. J. L. Bandfield, M. D. Smith, *Icarus* **161**, 47 (2003).
15. S. W. Ruff, P. R. Christensen, *J. Geophys. Res.* **107**, 5127 (2002).
16. P. R. Christensen *et al*., *J. Geophys. Res.* **105**, 9735 (2000).
17. S. W. Ruff, P. R. Christensen, P. W. Barbera, D. L. Anderson, *J. Geophys. Res.* **102**, 14899 (1997).
18. P. R. Christensen, Calibration Report for the Thermal Emission Spectrometer (TES) for the Mars Global Surveyor Mission, Mars Global Surveyor Project (Jet Propulsion Laboratory, Pasadena, CA, 1999).
19. M. D. Lane, P. R. Christensen, *Icarus* **135**, 528 (1998).
20. V. C. Farmer, *The Infrared Spectra of Minerals* (Mineralogical Society, London, 1974).
21. A. M. Baldridge, J. D. Farmer, J. E. Moersch, *J. Geophys. Res.* **109**, E12006 (2004).
22. M. T. Zuber *et al*., *J. Geophys. Res.* **97**, 7781 (1992).
23. J. B. Bandfield, *Nature* **447**, 64 (2007).
24. M. A. Presley, P. R. Christensen, *J. Geophys. Res.* **102**, 6551 (1997).
25. F. D. Palluconi, H. H. Kieffer, *Icarus* **45**, 415 (1981).
26. G. W. Brass, *Icarus* **42**, 20 (1980).
27. P. L. Knauth, D. M. Burt, *Icarus* **158**, 267 (2002).

28. We are grateful to the members of the THEMIS team at Arizona State University and the Mars Odyssey team at the Jet Propulsion Laboratory. We thank K. Nowicki for help with THEMIS data processing and M. Lane for the use of chloride samples and spectra. We also thank our anonymous reviewers for insightful, thorough, and constructive comments. Funding for this work was provided by NASA grant NNX06AE15G and the Mars Odyssey Science Office. Funding for V.E.H. was provided by grants from the Mars Odyssey Participating Scientist, the Mars Data Analysis, and the Planetary Geology and Geophysics programs.

Supporting Online Material

www.sciencemag.org/cgi/content/full/319/5870/1651/DC1
Materials and Methods
Figs. S1 and S2
References

18 September 2007; accepted 28 January 2008
10.1126/science.1150690

Sulfur and Chlorine in Late Cretaceous Deccan Magmas and Eruptive Gas Release

Stephen Self,* Stephen Blake, Kirti Sharma, Mike Widdowson, Sarah Sephton

Large-volume pāhoehoe lava flows erupted 67 to 65 million years ago, forming the Deccan Traps, India. The impact of these flood basalt eruptions on the global atmosphere and the coeval end-Cretaceous mass extinction has been uncertain. To assess the potential gas release from this volcanism, we measured sulfur and chlorine concentrations in rare glass inclusions inside crystals and on glassy selvages preserved within lavas. Concentrations range from ~1400 parts per million of S and 900 parts per million of Cl in inclusions down to a few hundred parts per million in the lava. These data indicate that eruptions of Deccan lavas could have released at most 0.103 weight % of S, yielding up to 5.4 teragrams of SO_2 per cubic kilometer of lava. A more conservative estimate is 0.07 weight % of S and 0.04 weight % of Cl, yielding 3.5 teragrams of SO_2 and 1 teragram of HCl for every cubic kilometer of lava erupted. The flows were very large in volume, and these results imply that huge amounts of S and Cl gases were released. The environmental impact from even individual eruptions during past flood basalt activity was probably severe.

Earth's most voluminous subaerial volcanic eruptions, both individual events and groups of closely spaced eruptions, happened during the formation of flood basalt provinces (*1*, *2*). These eruptions would have had a widespread environmental impact only through the release of gases, primarily S and Cl and possibly F (*3*). Of these, S gas releases are important in modern basaltic eruptions for causing atmospheric sulfate aerosol clouds, with well-documented climatic, weather, and other environmental effects (*4*), the distribution and severity of which have been replicated by modeling (*5*). By contrast, amounts of CO_2 released to the atmosphere even by flood basalt volcanism are thought to have been insufficient, when compared to the natural atmospheric reservoir, to have caused noticeable radiative effects (*2*, *6*). However, missing from these considerations have been directly measured data from the lavas that would constrain the amount of gas added to the atmosphere. The S and Cl contents of the magmas can be assessed indirectly by using a petrologic method (*7*, *8*) that has been validated by satellite-based measurements of SO_2 from recent eruptions of basaltic magma (*9*).

Here, we present direct determinations of S and Cl in glass inclusions in crystals in ancient basaltic lavas of the late Mesozoic, ~67 to 65 million years ago (Ma), Deccan flood basalt

Chloride-Bearing Materials in the Southern Highlands of Mars

M. M. Osterloo *et al.*

Science **319**, 1651 (2008);
DOI: 10.1126/science.1150690